Verification and Clearance of a Flight Control System for High Altitude Long Endurance Aircraft

Christian Weiser
German Aerospace Center (DLR)
Institute of Flight Systems
82234 Weßling
christian.weiser@dlr.de

Abstract—**This paper presents a three-step clearance process for flight control software. As a novelty, grid-based non-linear closed-loop simulation testing has been added within a unit test framework as a validation step. This new feature allows developers to assess compliance with requirements quickly on a very detailed level. Within this work, the extensive testing and the validation implemented for this unit testing framework are presented. Based on high-fidelity closed-loop simulation scenarios, the unit tests, including actuator and sensor dynamics, cover all nominal flight, disturbance, and fault conditions. Furthermore, test coverage is addressed and investigated as an indicator of the test framework quality. In the second and third steps, optimization-based clearance methods and Monte-Carlo simulation techniques assess the performance of the flight control laws in the presence of a worst-case aerodynamic parameter variation. The Monte Carlo simulation validates the worst-case scenario over the entire flight envelope and for all gust disturbance scenarios considered. The presented application example is the German Aerospace Center's High Altitude Long Endurance (HALE) platform HAP-ALPHA, which is used to illustrate all steps of the presented validation and verification (V&V) framework. The design and development of the flight control software development for the HALE aircraft has been discussed in previous work and has the novelty of considering the aircraft's flexible modes for the primary flight control design. The V&V framework assures compliance with functional, performance, and software quality requirements, allowing entry into an aircraft's flight testing phase.**

TABLE OF CONTENTS

1. INTRODUCTION

A flight control system has been developed for the German Aerospace Center (DLR) uncrewed High Altitude Long Endurance (HALE) aircraft project HAP-ALPHA, and the need for a validation framework is the primary motivation for this work. The DLR HALE project was launched to conduct satellite-like missions, e.g., surveillance and earth observation with optical and radar payloads at a much lower cost

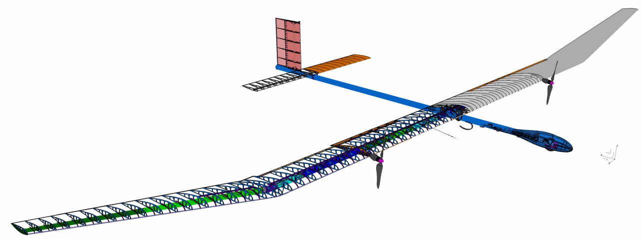

Figure 1: **HALE aircraft structure (©DLR).**

than low Earth orbit satellites [1]. One key advantage is the ability to conduct continuous observation of one location or a change of observation location, which is possible at low cost with the HALE aircraft in contrast to a satellite. Additionally, the opportunity to use multiple aircraft exists to cover more expansive areas or, e.g., provide telecommunication services for remote areas within a relatively short time. The DLR HALE aircraft is projected to fly solar- and battery-powered at an altitude between 60,000-80,000 ft with a payload of 5 kg. The wing span is approximately 27 meters, and the total take-off weight is projected at 136 kg. The aircraft's expected average mission duration ranges from 60 to 90 days. Limiting factors are the available solar energy in higher geographical latitudes and practical considerations, such as the maximum number of flight hours between scheduled maintenance. However, the available solar energy would theoretically allow an unlimited mission duration in certain latitudes. The current aircraft design is shown in Figure 1.

The design and development of the flight control software for the HALE aircraft has been discussed in various previous works, e.g., [2], [3], [4]. The control system design's principal novelty is the special aircraft configuration type and the consideration of the aircraft's flexible modes for the primary flight control design. For the development of the flight control functions, a requirement-based design has been chosen [2]. The functional requirements were developed according to standards and project specifications, e.g., the ability to operate in an augmented, piloted mode and fully autonomous operations with flight path vector guidance supplied by a Flight Management System (FMS).

The validation and verification (V&V) process presented here generally holds for any flight control law development and ensures compliance with requirements and tests for robustness whilst keeping the computational and implementation efforts on a level that can be handled in a scientific context

979-8-3503-5597-0/25/$31.00 ©2025 IEEE

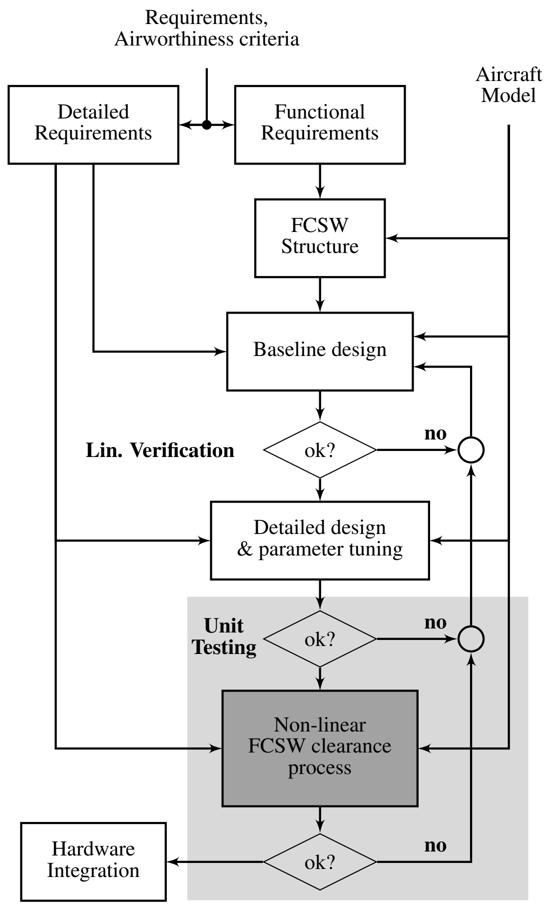

Figure 2: **Flight control design process graph.**

with small teams. The sketch in Figure 2 shows the process where the V&V procedure enters the complete Flight Control Software (FCSW) design process. The process is to be read from top to bottom, starting with functional and detailed performance requirements, which result in the FCSW structure. After tuning this structure with linear models and passing the linear verification process, the detailed controller design and tuning are executed, as illustrated in, e.g., [4]. At this stage, the non-linear V&V process, which is the topic of this paper, sets in (gray area in Figure 2). Finally, after passing the V&V process, hardware integration and flight testing are terminal steps.

For the design of the V&V toolchain, previous works on FCSW validation have been analyzed, e.g., robust and optimization-based clearance applied in [5] and a summary of certification benchmark processes in the industry [6]. As a first novelty, unit tests have been established to obtain a quick overview of the compliance with actual requirements. The unit tests can be seen as a grid-based analysis that systematically validates the control algorithm over the design envelope in nominal conditions, as well as disturbance and fault scenarios. It also automatically evaluates the design requirements.

Furthermore, worst-case search [7] is identified as a helpful tool that can increase confidence in the closed-loop system performance at a relatively low computational cost. This anti-optimization and a subsequent Monte-Carlo (MC) simulation are employed to test the robustness of the flight control laws. Moreover, identify critical aerodynamic uncertainties in combination with all valid operating points and disturbance scenarios. Furthermore, all simulations are carried out in the presence of sensor delays and noise.

Section 2 gives a brief overview of the modeling of the flexible HALE aircraft model and the control design. It also presents the closed-loop simulation framework, which is used for the V&V of the FCSW. Section 3 presents the proposed clearance strategy for FCSW and gives an overview of the simulation types used. The following sections explain three steps, including their practical application on the HALE example: Section 4 presents the software-in-the-loop (SIL) scenarios (unit tests) for FCSW clearance. It also focuses on the techniques to explain the automated collection and evaluation of the test results. Furthermore, additional aspects, such as model coverage testing, are addressed, rounding off the validation aspects. The description and evaluation of an anti-optimization-based search for an (aerodynamic) worst-case parameterization follows in Section 5. Finally, the MC simulation setup in Section 6 assesses the worst cases.

2. HALE Flight Control Software

For the design of the FCSW, a flexible flight dynamics model has been implemented based on the model data in references [8], [9], [10]. The model uses standard flight mechanics equations of motion [11] as implemented, e.g., in the DLRs VarLoads toolchain [12].

The rigid part of the non-linear equations of motion is defined as

$$\begin{bmatrix} m_\mathrm{b}(\dot{\mathbf{V}}_\mathrm{b} + \boldsymbol{\Omega}_\mathrm{b} \times \mathbf{V}_\mathrm{b} - \mathbf{T}_\mathrm{bE}\,\mathbf{g}_\mathrm{E}) \\ \mathbf{I}_\mathrm{b}\dot{\boldsymbol{\Omega}}_\mathrm{b} + \boldsymbol{\Omega}_\mathrm{b} \times (\mathbf{I}_\mathrm{b}\boldsymbol{\Omega}_\mathrm{b}) \end{bmatrix} = \boldsymbol{\Phi}_\mathrm{bg}\mathbf{P}_\mathrm{g}^\mathrm{ext}, \tag{1}$$

with the aircraft's mass m, its moment of inertia $\mathbf{I}_\mathrm{b}$, and the linear and rotational velocities $\mathbf{V}_\mathrm{b}$, $\boldsymbol{\Omega}_\mathrm{b}$. The flexible equation of motion is defined as a second-order linear equation of the form

$$\mathbf{M}_\mathrm{ff}\ddot{\mathbf{u}}_\mathrm{f} + \mathbf{D}_\mathrm{ff}\dot{\mathbf{u}}_\mathrm{f} + \mathbf{K}_\mathrm{ff}\mathbf{u}_\mathrm{f} = \boldsymbol{\Phi}_\mathrm{fg}\mathbf{P}_\mathrm{g}^\mathrm{ext}, \tag{2}$$

with the mass matrix $\mathbf{M}_\mathrm{ff}$, damping matrix $\mathbf{D}_\mathrm{ff}$, and stiffness matrix $\mathbf{K}_\mathrm{ff}$. The variable $\mathbf{u}_\mathrm{f}$ denotes the modal displacement of the structural nodes of the model. The equations (1) and (2) have the external forces and moments $\mathbf{P}_\mathrm{g}^\mathrm{ext}$ on the right-hand side. These are calculated from the aerodynamic and propulsion loads. This procedure is described in more detail in [12]. Additionally, via the force summation method [13], load recovery can be executed. This enables the analysis of structural loads at various cut-points within the aircraft in post-processing. Additionally, the load monitoring stations can be set as an output during linearization. This possibility can be used later in the V&V framework to determine the influences of the controller on the peak structural loads.

The above-presented non-linear model serves for:

1. generating linear models of the form

$$\begin{bmatrix} \dot{x} \\ \hline y \end{bmatrix} = \left[\begin{array}{c|cc} A & B_u & B_d \\ \hline C & D_u & D_d \end{array}\right] \begin{bmatrix} x \\ \hline u \\ d \end{bmatrix} \tag{3}$$

which are used for linear control design using robust control design methods. The vector x denotes the state vector, including relevant rigid body and flexible states, u is the

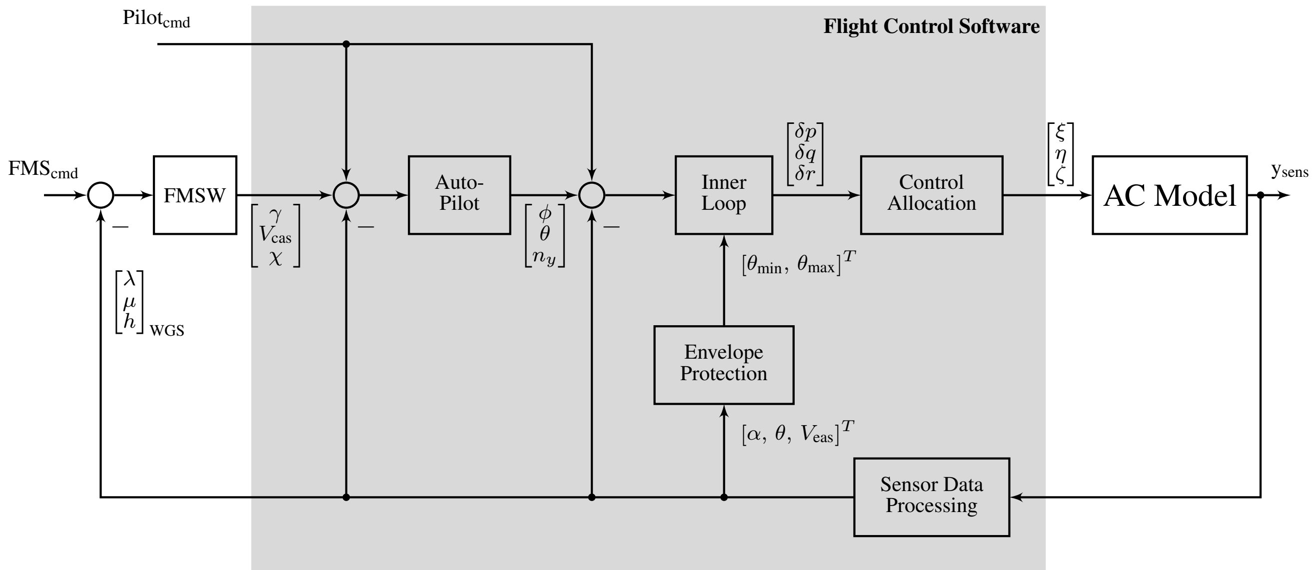

Figure 3: **Flight control architecture diagram.**

control input, i.e., control surface deflection angles, y denotes the output vector and d is the disturbance vector added after linearization.

2. The non-linear model is used for simulations in the software-in-the-loop (SIL) environment to evaluate the control laws.

Starting the process chart in Figure 2 from top to bottom, besides the model data, the requirements for the FCSW are needed. These can be derived from standards such as, e.g., SAE AS94900 [14] and an analysis of the flight dynamics. The control structure is selected as a cascaded architecture [2] (gray background area in Figure 3), consisting of an inner loop, which tracks the roll attitude Φ and pitch attitude Θ. The outer cascade is the auto-pilot (AP) which follows commands in the flight path angle (FPA) γ, equivalent airspeed (EAS), and track angle χ. On the right-hand side, not included in the control software, AC MODEL denotes the non-linear, flexible aircraft dynamics including sensors and actuators. For the control design, the actuators and sensors are simplified as second-order dynamics and a delay approximation. From Figure 3 the following four main control modes, which will be assessed in the V&V toolchain, can be derived:

1. Manual Mode: the pilot command is mapped to the control surfaces, and no protection algorithms are active.

2. Augmented Mode: the inner loop rate-command-attitude-hold (RCAH) control law is active, and the pilot command is interpreted as pitch and roll rate command.

3. Flight Path Mode: the autopilot controls the flight path vector with the entries airspeed, FPA, and course angle command ($[V, \quad \gamma, \quad \chi]^T$), defined by the operator.

4. Managed Mode: an FMS, which is not part of the FCSW, controls the aircraft trajectory and provides the flight path vector command.

Additional controller components depicted in Figure 3 are the control allocation, which maps the inner loop command to the control surfaces. In this case, a fixed allocation is chosen, since the minimal weight requirement of the aircraft causes hardly any redundancy in the HALE which would allow dynamic re-configuration. The Envelope Protection, however, tracks the airspeed and angle of attack (AoA) during Augmented Mode operation and dynamically adjusts the pitch attitude limits in the inner loop according to the current airspeed vector. This function can be disabled as soon as the airspeed is managed by the autopilot. The design of the inner loop and autopilot control laws used structured H_∞ control and has been presented in [2]. The linear verification, shown in Figure 2, has also been passed in the previous publications [2], [3], [4] and this work continues at the stage of non-linear verification.

Simulation Framework

Both simulation analysis techniques use a high-fidelity aircraft model of the DLR HALE aircraft. Figure 4 shows the closed-loop simulation model which is an interconnection of the described aircraft model with the FCSW. This model has been generated using the non-linear flexible aircraft dynamics presented in (1) and (2). Furthermore, an actuator model is added, which is provided by the manufacturer [15] and sensors, using a second-order transfer function for the mechanical components and a proportional controller approximation of the motor current controller. The propulsion system is modeled as a PT-1 motor and the rotational speed n is converted to thrust via a detailed look-up table providing the thrust coefficient based on the propeller advance ratio $J = \frac{V_a}{n\,D}$ using the true airspeed V_a and the propeller diameter D. Sensor models are added to estimate the delay and noise of the original system so that an overall realistic high-fidelity aircraft model is achieved.

Disturbance Modeling

One important aspect of V&V of the closed-loop behavior of the HALE aircraft is the reaction to worst-case discrete

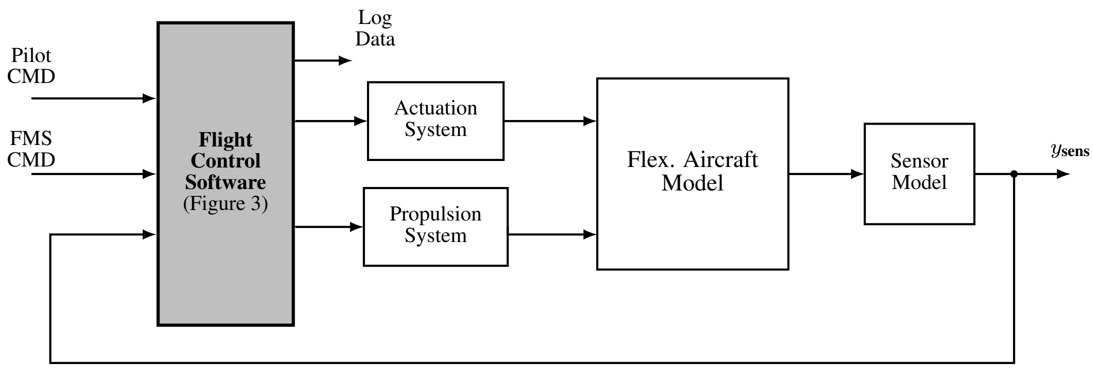

Figure 4: **Block diagram of SIL simulation environment.**

gusts. For defining such, the gust definition described in the EASA CS25 specification [16] is used and slightly adapted: the spatial wind velocity profile u_g of the discrete gust (1-cos shape) is defined by the certification requirements in CS 25.341 [16]:

$$u_g = \frac{U_{\text{ds}}}{2}\left(1 - \cos\left(\frac{2\pi x}{2H}\right)\right), \tag{4}$$

where U_{ds} is the gust design velocity. H is the gust gradient, i.e., the distance parallel to the aircraft's flight path for the gust to reach its peak, and x is the distance penetrated by the gust. As the DLR HALE flies at very low equivalent airspeed, the gust gradient H has been slightly adjusted to lower values (5 to 100 m) vs. 9 to 107 m in the CS25. For the HALE aircraft, the gust design velocity is reduced by 50% to account for the fact that flights will only be carried out under close weather surveillance and that the planned flight time in the aircraft life is very low compared to a regular transport aircraft. This corresponds to the V_D (dive speed) requirement in the CS25. The design gust velocity is defined as

$$U_{\text{ds}} = U_{\text{ref}} F_g (\frac{H}{107})^{1/6}, \tag{5}$$

where F_g is the flight profile alleviation factor, which is for sea level $F_g = 0.84$ in the case of the HALE according to [16], [17] (design loads) and increases linearly to one at maximum operating altitude z_{mo}. U_{ref} is selected as 0.5 times the specification value at sea level and increases to the CS25 value at higher altitudes ($> 10\,\text{km}$). The calculation of the aerodynamic loads due to the discrete gust is implemented as presented in [18], [19]. Furthermore, the 1-cos gust is considered in different directions ζ_g, namely vertical gusts from positive and negative z-axis, lateral gusts in the aircraft y-direction, and gusts perpendicular to the winglets. For the anti-optimization and MC simulation, all values for ζ_g between $-\pi$, and π are permitted.

Finally, additional disturbance in the form of continuous turbulence is considered for the disturbance rejection tests. The continuous turbulence is modeled via the Dryden/Karman Wind Turbulence model [20], [19], where the power spectral densities for certain turbulence intensity levels are given. A detailed analysis of the interaction of the HALE autopilot with worst-case turbulence has been investigated in [3]. For the HALE application, low (true) airspeed near the ground and low inertia and total energy do not allow more than light turbulence for take-off and landing phases. This can be accomplished via good meteorological forecasts and decision-making. However, the resulting restrictions, especially on wind conditions, significantly limit the operational days in central Europe and most other regions For high altitudes, e.g., cruise flight at altitudes greater than 15 km, moderate turbulence is selected as a design requirement.

3. PROPOSED FCSW CLEARANCE PROCESS

This work proposes a process with three steps for the non-linear model-based clearance of flight control laws. This process assumes that the control law has been tuned in the linear domain, as shown in Section 2 and Figure 2. Further, it is assumed that linear clearance, e.g., performance metrics and stability based on disk margins, has been checked. A summary of the proposed steps is given below, whilst the different steps are explained in detail in Sections 4 to 6, using the DLR HALE platform as an example application. The process is graphically illustrated in Figure 5.

1. SIL unit testing: the non-linear closed-loop simulation model is introduced in the first step. A test matrix of all nominal flight conditions, control modes, operator inputs, and worst-case disturbances is determined. For each of the test scenarios, one simulation-based unit test is generated. These tests can automatically be triggered after each major change and for each release candidate of the FCSW algorithms. The idea behind these tests is to obtain an overview of the FCSW closed-loop performance under all possible circumstances and identify critical operating conditions quickly. Different types of code coverage can be used as a metric for the completeness of the unit test matrix.

2. Worst-case search via anti-optimization is used as a second step to check the performance over the full envelope in the presence of worst-case disturbance and parameter uncertainties following recommendations in [7]. Potential critical sets of (uncertainty) parameter combinations can be identified with high reliability.

3. As a final step, a MC simulation using the worst-case parameter combinations obtained in the anti-optimization is executed. The above can be used to back up the worst-case search. For each of the identified worst-case parameter sets, a MC simulation run is executed where the operating point and external disturbance parameters are varied. The result can provide numerical proof of the anti-optimization, including a quantitative overview of the risk at which the identified worst-case conditions can occur.

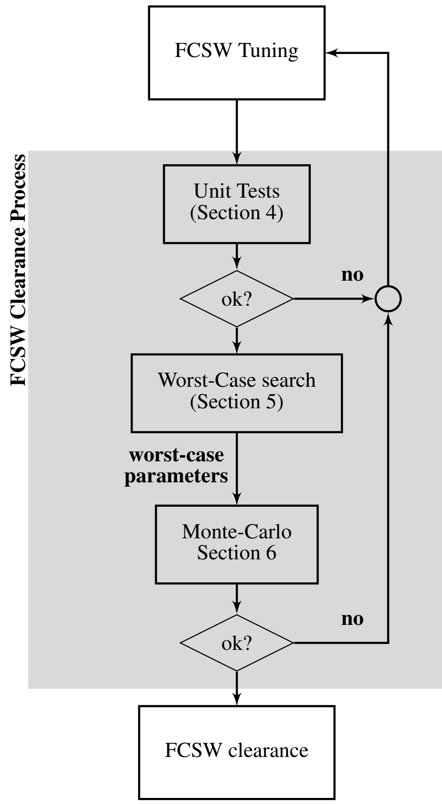

Figure 5: **Schematics of proposed clearance process.**

4. UNIT TESTS

For each controller function, test cases are developed that test the nominal behavior and the aircraft response under disturbances.

Unit Test Definitions

The test cases are listed in Table 1 and can be divided into three main categories: a) Command, b) Disturbance, and c) Failure-related simulations. Columns 3-7 in Table 1 list the relevant active controller modes. $\mathbf{RCAH_{lon}}$/$\mathbf{RCAH_{lat}}$ denotes that the inner loop RCAH system is active (Augmented Mode). On top of this, the autopilot can be activated in various mode combinations. The relevant combinations for analysis were selected to be:

1. Speed by pitch, i.e., the autopilot controls airspeed via the pitch RCAH inner loop, while the thrust is controlled manually.

2. Combined speed and vertical autopilot: FPA and airspeed are controlled via the control variables pitch attitude and thrust in this mode. For this mode, there exist two sub-configurations:

(a) The operator directly commands the FPA.

(b) The altitude command is selected as a control variable. An additional proportional loop handles the altitude control error for this setting and provides the FPA command.

3. Course angle (course over ground) is controlled.
This control loop has a relatively simple proportional architecture, although moderate winds, which may be of similar magnitude as the airspeed, can drive the computations into limits (e.g., flying ”backward” when airspeed and ground speed vector have an angle greater than $90\mathrm{deg}$).

4. A combination of the course angle mode and the altitude/airspeed mode is tested.

5. FMS operation: this mode is similar to the combination of course and altitude/airspeed mentioned above, but commands are not obtained from the operator interface but from the FMS interface with an additional input for the cross-track distance Δy which denotes the potential offset from a course line.

In Table 1, ”X” denotes that the mode is permanently active. If noted in brackets, the case listed in the table has multiple sub-cases with all valid mode combinations of the modes marked with ”(X)”. This means if the AP modes are all three marked as ”(X)”, five different test scenarios result (instead of 2^3), as not all combinations are valid or relevant modes on the aircraft. The allowed mode combinations are guarded by a state machine within the FMS.

In the first part of Table 1, the nominal performance of the controller is assessed in each mode. These are the RCAH inner loop controller, which is checked for correct enabling behavior, along with response characteristics in pitch and roll. The unit test metrics are implemented as an automated assessment of the controller performance to obtain a fast overview of the controller performance in different scenarios. For the step responses, the desired response characteristics are the rise time (in seconds), overshoot (%), and tracking accuracy (absolute). These values are specified in the performance requirements (see Figure 2) and are derived from project specifications and handbooks ([20], [14]). They can also be automatically assessed post-simulation and be shown as a simple pass/fail value in the test overview (see Figure 7). The step responses in the RCAH and AP command variables are tested at V_{min}, V_{max}, and at three different altitudes from sea level to 80,000 ft. The step responses and their metrics in detail are:

1. The step response in V_{eas} is observed in the two relevant AP modes: one with pitch control only and one with the thrust controlled manually. The second setting tests the velocity step with thrust control active. Both settings test a 1 m/s step for tracking evaluation and a step towards maximum and minimum airspeed against rise time and overshoot.

2. FPA command: positive and negative steps are implemented, of magnitude $1\,\mathrm{deg}$, to evaluate the tracking requirements, but also of the maximum allowed value to validate the speed priority and AW mitigation of the longitudinal AP.

3. Altitude command: one positive and one negative step in altitude are implemented for this test case. The limit in FPA and the behavior in thrust saturation (maximum and idle thrust) can be observed, together with the AW mitigation of the longitudinal AP.

4. Heading/course command: for this step response, one test case selects the heading and another course tracking mode. In one mode, the step is commanded in a positive direction, one time in a negative direction, explicitly passing the $360\,\mathrm{deg}\,/0\,\mathrm{deg}$ crossing.

For the disturbance tests, the scenarios listed in Table 1 are described in detail:

1. Gust encounters: for all valid controller configurations, 1 -

Table 1: **Overview of SIL test scenarios.**

	Test Name	$\mathbf{RCAH_{lon}}$	$\mathbf{RCAH_{lat}}$	$\mathbf{AP_{speed}}$	$\mathbf{AP_{lon}}$	$\mathbf{AP_{lat}}$	**Desired Outcome**
Command	Enable RCAH	X	X				Check transient-free RCAH enabling
	Step pitch	X	X				Evaluation of step response characteristics
	Step roll	X	X				(rise time, overshoot)
	Pitch anti-windup (AW)	X	X				Evaluation of pitch anti-windup
	Roll AW	X	X				Evaluation of roll anti-windup
	Enable AP	X	X	(X)	(X)	(X)	Check transient free AP enabling
	Step EAS	X	X	(X)	(X)		Evaluation of velocity step characteristics
	Step EAS max/min	X	X	(X)	(X)		No overshoot of limits, no windup
	Step FPA	X	X	X	X		evaluation of FPA step characteristics
	Step heading/course	X	X			X	Step tracking characteristics of lateral AP
Disturbance	1-cosine gust vertical	X	X	(X)	(X)	(X)	
	1-cosine gust lateral	X	X	(X)	(X)	(X)	Check if all parameters remain
	1-cosine gust winglet	X	X	(X)	(X)	(X)	bounded/RMS amplitudes are smaller than
	Span-wise distributed gust (DARPA)	X	X	(X)	(X)	(X)	in open loop
	Continuous turbulence	X	X	(X)	(X)	(X)	
	Constant wind	X	X	(X)	(X)	X	Check behavior with wind velocities
	Wind velocity ramps	X	X	(X)	(X)	X	exceeding climb/sink rates or airspeed
Faults	Single aileron stuck at zero	X	X				
	Single aileron hard-over	X	X				
	Rudder stuck at zero	X	X				
	Rudder hard-over	X	X				Check if the aircraft remains
	Elevator stuck at zero	X	X				controllable/no sudden departure occurs
	Air data failure	X	X	(X)	(X)		No controller-induced departure in less than 30 s

cosine gusts, as defined in Section 2, are set as inputs. Three gust gradients (short, medium, long) and four angles (from negative and positive z-direction, lateral and perpendicular to the winglet) are selected for these unit tests.

2. Continuous turbulence: similar to the 1-cosine worst-case gust scenario, continuous turbulence, as defined in the MIL handbook [20], is set as input. The turbulence intensity is set to "light" for lower altitudes (corresponds to a probability of exceedance of 10e-2) and moderate for high altitudes ($>$ 20 km).

3. Constant wind fields and wind shear in all three directions (in earth-fixed coordinates). This wind scenario does not influence the aircraft dynamics, as fast changes are already assessed in the gust simulations. Instead, this scenario specifically targets the navigation calculations with cases where the wind and airspeed vectors are in opposite directions, resulting in low ground speed or ground speed vectors deviating by more than 60 deg from the body x-axis.

All scenarios are executed for three different altitudes and four velocities ranging from close to stall up to maximum allowed airspeed. For the assessment of all scenarios, compliance with the flight envelope parameter limits is checked as a further metric. These parameters are listed in Table 2.

In the DISTURBANCE tests in Table 1, the never-exceed limits ($[\mathrm{Min, Max}]_{\mathrm{wc}}$) from Table 2 are used, while in the Command section, the nominal (nom) limits are used. Furthermore, the same simulation scenario is always run in the open loop mode for the disturbance test cases, i.e., with no controller active

[2]Nominal limits are determined by the envelope protection/autopilot.

Table 2: **Flight envelope parameter limits.**

	$\mathbf{[Min, Max]_{nom}}$	$\mathbf{[Min, Max]_{wc}}$
V_{eas}	[9, 11]	[6.5, 14.5] m/s
Θ	-[2]	[-15, 15] deg
Φ	[-10, 10] deg	[-15, 15] deg
p	-	[-2.5, 2.5] deg/s
q	-	[-23, 23] deg/s
r	-	[-10, 10] deg/s
n_{y}	[-0.03, 0.03] g	[-0.1, 0.1] g
n_{z}	[0, 1.5] g	[-1, +2] g
$\dot{\chi}$	-	[-5, 5] deg
$M_{\mathrm{x,\,WR}}$	-	[-2e3, 2.8e3] Nm
$M_{\mathrm{x,\,VT}}$	-	[-110, 110] Nm

but with the same disturbance input. Post simulation, the responses of open and closed-loop are compared and assessed if, for relevant aircraft parameters, the induced disturbance energy is less in closed-loop than in open loop. If this criterion is not met, the respective test is marked as "failed". All of the criteria mentioned above can be linked to controller requirements. Consequently, the unit test report can be used as a validation report against the design requirements in Figure 2.

One detailed example for the test discussion is the bump-less transfer. This is one of the major functional requirements for smooth switching during flight operations. For this reason, the ENABLE test cases (first line in Table 1) have been implemented. The example evaluation of this test case is presented in Figure 6. The RCAH control system is activated from t=5 s to t=10 s and from t=15 s (green areas in Figure 6. At t=5 s, the pitch signals and elevator command remain steady, and

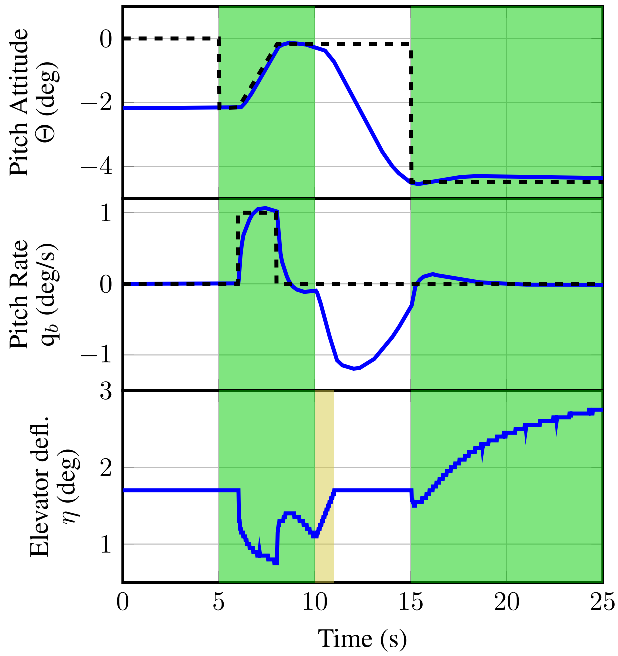

Figure 6: **Result of ENABLE test case.**

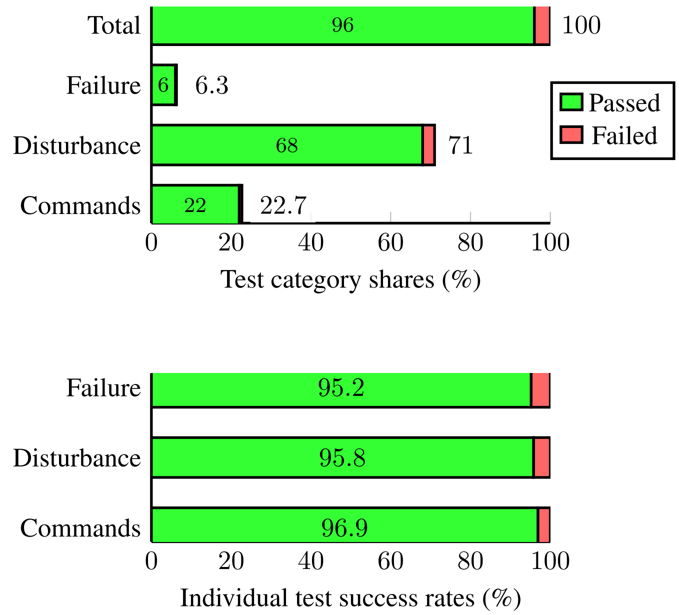

Figure 7: **Unit test result overview.**

no change occurs as intended. After t=6 s, a 1 deg pitch up command is given, which results in a 2 deg pitch attitude (Θ) change. After disabling the controller at t=10 s, the elevator returns to the pilot's stick position within 1 s (the initial trim setting at simulation start), marked in yellow in the lower diagram of Figure 6. This results in a phugoid movement of the aircraft, which is immediately stopped after re-enabling at t=15 s. This enabling case can also be automatically assessed by test criteria. After activation, the error between pitch attitude command and pitch attitude shall be less than 0.2 deg, for instance, and there shall be no overshoot.

Finally, failure scenarios considering actuator and air data faults are added, as listed in Table 1. The hard-over and stuck scenarios are simulated for the aileron and rudder, while the elevator is only simulated as stuck. The elevator hard-over would lead to a loss of aircraft immediately. The air data faults target the airspeed and altitude measurement, which are critical for scheduling the controller gains. Again, in all test cases, the maximum variable limits defined in the performance requirements are checked (see Table 2). The design of failure and wind shear tests was mainly driven by the analysis of code and decision coverage within the FCSW. The coverage reports indicated that especially related to decision coverage, failures, and adverse conditions are necessary to test all paths within the software, e.g., the behavior of scheduling variables at airspeed above or below the operational envelope.

Unit Test Results

The test cases presented above can be executed in parallel, and the results are automatically evaluated against the mentioned performance and robustness metrics. This evaluation takes about two hours on a standard processor with 16 cores and 128 GB RAM. Thus, it is feasible to execute the procedure after each significant change. For the DLR HALE example, the automated report identifies failure rates of approximately 4-5% in the test runs, as seen in Figure 7.

These failed test cases were analyzed by category, as shown in Figure 7. The failed tests in the command category are analyzed the most since these potentially cause non-compliance of the FCSW with the requirements. In several cases, though, (planned) interventions of the envelope protection software were detected as non-compliance with the tracking performance. This led to improvements in the automated evaluation algorithms, such that they can handle more complicated test cases, which also holds for, e.g., command responses or gust encounters at the edges of the flight envelope. Future development aims to improve the automated test evaluation to avoid these false negatives. This can be achieved by refining the test criteria after analysis of the false negatives. Therefore, once before final clearance, a manual check of passed tests to find false positives should be conducted.

However, it is assumed that false positives (tests meeting all analysis criteria, even though the simulation violates boundaries) are presumed to be much less likely than false negatives (simulations detected as failed, even though the closed-loop model behaves as intended). This assumption is driven by the fact that all envelope parameters are checked, and thus, if any oscillations or instabilities occur, at least one of the envelope testing criteria would fail.

For the disturbance tests, which contribute to most failed scenarios, the critical test cases have been identified as gust simulations. Here, the aircraft reaction violates the flight envelope quicker than the FCSW can recover with full control surface deflection. As a consequence, the operational envelope regarding rare gust and operating point combinations might need adaptation sporadically.

To ensure that all parts of the HALE FCSW algorithm are tested at least once, model coverage is collected during the unit tests. The coverage tests can be split into execution, decision, and modified condition/decision coverage (MCDC). With this analysis, the current test setup for the HALE in Table 1 reached 100% coverage in all three metrics.

Table 3: Allowed parameter variations.

	Parameter Name	Value
δC_{lp}	Roll damping	[-15, 15] %
δC_{nr}	Yaw damping	[-15, 15] %
$\delta C_{\text{l}\xi}$	Roll moment by aileron	[-15, 15] %
$\delta C_{\text{n}\zeta}$	Yaw moment by rudder	[-15, 15] %
$\delta C_{\text{m}\eta}$	Pitch moment by elevator	[-15, 15] %
δC_{mq}	Pitch damping	[-15, 15] %
δx_{cg}	C.o.g. variation in x	[-0.1, 0.1] m
h	Altitude	[0, 80000] ft
V_{trim}	Equivalent Airspeed	[8, 12] m/s
H_{gs}	Gust gradient	[5, 100] m
ζ_{gs}	Gust angle	[-90, 90] deg

5. Worst-Case Search via Anti-Optimization

After passing the unit testing framework, a worst-case search is performed for the closed-loop system. For this test setup, only the RCAH inner loop controller is active, as it is intended, that only this controller will mitigate high-frequency or discrete disturbances. Furthermore, the interaction of gust and turbulence with the AP has sufficiently been tested in the previous unit test section and the further tests mainly aim at robustness to model uncertainty which is most critical in the inner control loops. Thus, this setup aims at finding a worst-case combination of gust disturbance parameters and aerodynamic model uncertainties. The available uncertainties are aerodynamic parameters and the Center of Gravity (CoG) position, listed in Table 3. These parameters can be varied within the shown limits and use a normal distribution in the MC simulation. Additionally, the already discussed gust parameters (H_{gs} and ζ_{gs}) and the operating point are used in the anti-optimization with an equal distribution.

For the worst-case search, the global optimization technique is used since this promises high reliability in finding weaknesses compared to gridding and MC approaches [7], [21]. Furthermore, this process does not add conservatism (in contrast to, e.g., linear methods such as μ-Synthesis), and the optimization approach is very flexible concerning the problem type. The worst-case parameter set found can be used to improve the FCSW parameters further.

Formulation of a Global Optimization Problem

For utilizing optimization methods the clearance problem has to be expressed as a scalar objective function $c(p, d)$ with optimization parameters p that are uncertain or varying during operation (e.g., aerodynamic coefficients, wind or aircraft mass, inertia, speed, height, etc.) and discrete conditions d (e.g., aircraft configuration, landing gear settings, etc.). The components of p are assumed to be bounded and continuously varying over known intervals, defining a hyper-box P. The clearance problem can now be formulated as a minimization problem. Let $c_0(d)$ be a lower acceptable value for c then

$$c_{\text{min}}(d) = \min_{p \in P} (c(p, d)) \tag{6}$$

is a measure for the clearance performance. We assume that the clearance requirement is fulfilled for condition d if $c_{\text{min}}(d) \geq c_0(d)$, otherwise the criterion is not cleared. For the worst-case search, the MOHGA algorithm available within the DLR Multi-Objective Parameter Synthesis (MOPS) toolbox [22] is used. MOHGA is primarily developed to solve multi-objective optimization problems, i.e., to find approximations of the Pareto front. For this, MOHGA applies a hybrid solution of a non-dominated sorting algorithm, similar to the NSGA-II algorithm described by Deb et al. [23], which is combined with a pattern search algorithm. In the case of constraints, infeasible solutions are always considered worse than feasible ones.

For the DLR HALE example, the following criteria are selected from the envelope parameters in Table 2 for the worst-case search:

- the maximum roll attitude $c_1 = \max(|\Phi|)$
- maximum load factor $c_2 = \max(n_z)$
- margin to never exceed airspeed V_{ne}, $c_3 = \max(\frac{V_{\text{eas}}}{V_{\text{ne}}})$
- margin to stall speed V_{s}, $c_4 = \max(\frac{V_{\text{s}}}{V_{\text{eas}}})$
- maximum vertical tail bending moment $c_5 = \max(|M_{\text{x, VT}}|)$
- maximum wing root bending moment $c_6 = \max(|M_{\text{x, WR}}|)$

The selection aims to check for critical conditions with regard to the integrity of the aircraft's structure and stall risk. All six criteria are formulated in a manner, such that low values are denoted as GOOD and thus the anti-optimization problem shall maximize each of the six criteria. The result of this anti-optimization problem for the HALE aircraft is shown in Table 4. Only for the load factor n_z, stall, and overspeed margin the limits could be violated by the algorithm (marked in red in Table 4). Table 5 shows the results for the violated criteria 2-4 in detail with their corresponding parameter values. The remaining criteria are omitted since they did not exceed the envelope limits during the worst-case search. Analyzing the parameter values in Table 5, for all three worst cases the aerodynamic uncertainties are almost all non-zero. This is expected and gives confidence, that worst-case performance will not occur during the lifespan of the aircraft in case the model uncertainty is less than the values shown in Table 5.

Table 4: Worst-case search results.

	Unit	WC value	Limit
$c_1 = \max(|\Phi|)$	deg	8.6	10
$c_2 = \max(n_z)$	g	2.39	2
$c_3 = \max(\frac{V_{\text{eas}}}{V_{\text{ne}}})$	-	1.08	0.99
$c_4 = \max(\frac{V_{\text{s}}}{V_{\text{eas}}})$	-	1.04	0.97
$c_5 = \max(|M_{\text{x, VT}}|)$	Nm	103	120
$c_6 = \max(|M_{\text{x, WR}}|)$	Nm	2700	2800

Table 5: Identified worst-case parameterizations.

	c_2 ($\mathbf{N}_z$)	c_3 ($\mathbf{V}_\mathbf{s}$)	c_4 ($\mathbf{V}_\mathbf{ne}$)
h (ft)	62e3	1.0e3	1.3e3
V_{trim} (m/s)	12.0	11.8	8.1
H_{gs} (m)	14	90	58
ζ_{gs} (deg)	-88	0	3
Δx_{cg} (m)	0.04	0.03	-0.02
δC_{lp} (%)	14.2	-13.3	10.3
δC_{nr} (%)	-4.3	14.5	-6.6
$\delta C_{\text{l}\xi}$ (%)	6.6	-10.7	-8.4
$\delta C_{\text{n}\zeta}$ (%)	-3.6	-11.4	-1.4
$\delta C_{\text{m}\eta}$ (%)	-10.4	-10.0	7.0
δC_{mq} (%)	7.5	-0.4	-10.3

Table 6: **Monte-Carlo simulation parameters.**

	Min	Max
h (ft)	0	80e3
V_{trim} (m/s)	8	12
Gust gradient H_{gs} (m)	5	110
Gust angle ζ_{gs} (deg)	-90	90

6. MONTE-CARLO SIMULATION

For the critical worst-case results found above in the anti-optimization step, the clearance process proposed in this work suggests, that individual MC runs are carried out using the worst-case parameterizations from Table 5. Furthermore, a MC run of the nominal model parameterization can be simulated for reference. The MC simulation parameters are the operational envelope parameters, e.g., altitude, airspeed, and gust (see Table 6). Furthermore, the MC simulation uses the same framework as the SIL unit tests and the anti-optimization. This is inspired by the idea of underlining the worst-case result from Section 5 with statistical data and providing confidence in the found worst-case. In the HALE example, the critical parameters are listed in Table 4: stall margin, maximum airspeed margin, and maximum load factor. The according worst-case parameterizations can be found in Table 5. With these parameters, three individual MC simulation runs with $n = 3,000$ simulations are carried out. Additionally, the same is executed for the nominal parameterization.

The results are depicted in Figure 8 and are displayed as cumulative density function (CDF)s. With this type of plot, the operational risk of experiencing a violation of the envelope can be assessed. It has to be noted, that the aircraft under test is meant to fly only very few hours (< 100 in the first version), and therefore the risk per flight hour which is acceptable is significantly higher than for commercial aircraft. Furthermore, in the case of this MC simulation campaign, all simulations are carried out under worst-case gust conditions. As a consequence, the plots in Figure 8 can be read as the risk per arbitrary worst-case gust encounter for the aircraft to violate its envelope parameter. Figure 8a evaluates the CDF for the maximum load factor criterion (c_2). In the figure, the parameterization (of aerodynamic and CoG offset) has no visible influence on the maximum load factor response. Thus, it can be concluded that this criterion can mainly be influenced by the gust parameterization in combination with the operating point of the aircraft. Since the result does not vary for the relatively different aerodynamic parameter configurations, it is not likely that further tuning of the FCSW could improve the probability of load factor exceeding in the presence of gust disturbance. This fits well with the unit test result in Section 4, where several disturbance tests under nominal conditions failed due to the gust input driving the aircraft into flight envelope violations before any control action can compensate. This is expected to disappear after introducing even more restrictive operational conditions for disturbance scenarios. Figures 8b and 8c show the CDFs of the over-speed and stall margins. For these two parameters, a difference in the CDF curves in Figure 8 is visible for the different aerodynamic and CoG parameter configurations. Nevertheless, only the worst-case parameter sets for stall and over-speed violate their respective envelope limits (i.e., violate the red areas in the plot). None of the four times 3,000 simulations (three worst-case parameter sets plus nominal configuration) exceeded any of the worst-case boundaries (vertical red dashed lines in Figure 8) found in the anti-optimization in Section 5.

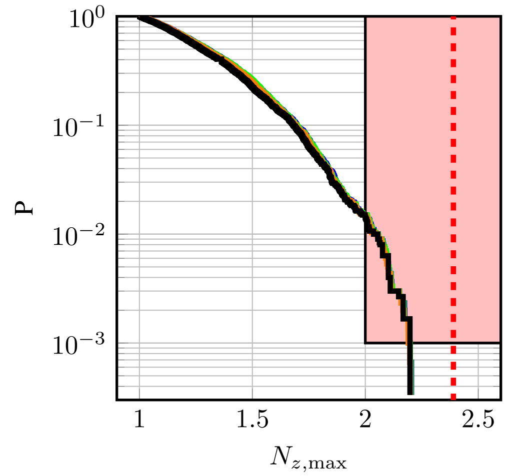

(a) **CDFs for N_z envelope border.**

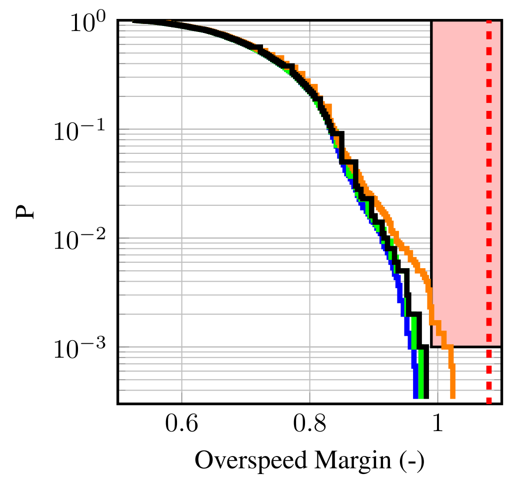

(b) **CDFs for V_{ne} envelope border.**

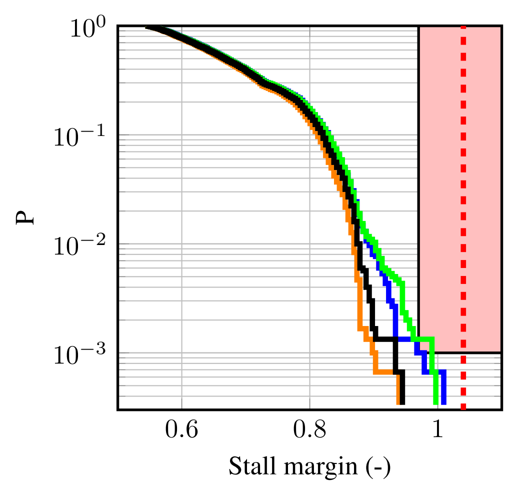

(c) **CDFs for V_s envelope border.**

Figure 8: **CDFs for worst-case parameterizations in N_z (▬), V_{ne} (▬), V_s (▬) and nominal (▬) parameter configurations; worst-case values from anti-optimization are dashed red lines.**

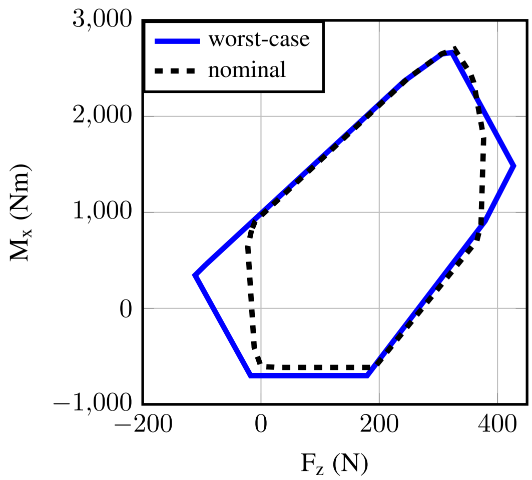

Figure 9: **Worst-case gust load envelope at the wing root.**

The number of 3,000 MC evaluations has been chosen to prove a failure probability $p < 1e-3$. Additionally, the MC results can be used to cross-check with the load envelope. For this purpose, the MC results of the maximum wing-root bending moment $M_{\mathrm{x,\,WR}}$ versus force in z-direction at the wing root F_{z} are evaluated and the convex hull of the values is depicted in Figure 9. The blue curve in Figure 9 evaluates the MC simulation using the worst-case parameterization for $N_{\mathbf{z,\,max}}$ and the black dashed curve evaluates the nominal model. The general shape of Figure 9 and its maximum values show good compliance with the loads analysis in [17] and suggest that even worst-case gusts in combination with aerodynamic parameter variations cannot cause structural loads above the structural design limits.

7. Summary

The presented V&V strategy shows an extensive campaign for a flight control system's non-linear, closed-loop assessment. The procedure focuses on providing high confidence in compliance with requirements at an acceptable cost in a scientific context. This means the framework can be implemented with a small team, and the clearance assessment takes relatively low time and computational resources ($< 1\,\mathrm{d}$ on standard PC) while using a combination of unit tests and optimization-based clearance processes. The introduced unit testing part assesses the functionality of all relevant control modes and inputs over the flight envelope. The target is to achieve 100% model coverage with 100% compliance for command test cases during nominal operation and $< 5\%$ failure rate for induced fault cases and worst-case disturbances. An anti-optimization-based worst-case search is used to find a worst-case set of aerodynamic uncertainty parameters that drive the closed-loop reaction to 1-cosine gust disturbances across the envelope borders. These worst-case results are finally assessed within the MC simulation, which ensures the controller's stability concerning the found worst-case model uncertainties in combination with operating point and disturbance parameters. The design has been proven as a practical example for the control design of a lightweight, flexible HALE aircraft. Test results identified that the load factor envelope is violated independently of model uncertainty, and the violation is only driven by disturbance parameters. As a result, the permitted gust disturbance shall be reduced such that the envelope limits are not exceeded.

Acknowledgments

This work was funded as part of the DLR-internal HAP-alpha project. The author thanks the colleagues at DLR Institutes of Aerodynamics and Flow Technology, Aeroelasticity, Flight Systems, Lightweight Systems, and Software Technology for providing model data, cooperation during hardware integration, and valuable discussions.

References

[1] F. Nikodem, "Overview of the DLR High Altitude Platform and scientific potential of the technology demonstrator HAP-Alpha," in *Deutscher Luft- und Raumfahrtkongress 2023*, 2023. [Online]. Available: https://elib.dlr.de/198509/

[2] C. Weiser and D. Ossmann, "Baseline flight control system for high altitude long endurance aircraft," in *AIAA SciTech Forum*. American Institute of Aeronautics and Astronautics, 2022.

[3] C. Weiser, D. Ossmann, and H. Pfifer, "Robust path-following control for high-altitude long-endurance aircraft," *Journal of Guidance, Control, and Dynamics*, vol. 46, no. 7, pp. 1416–1424, May 2023.

[4] C. Weiser, S. Schulz, A. Voß, and D. Ossmann, "Attitude control for HALE aircraft considering structural load limits," in *AIAA SciTech Forum*, 2023.

[5] G. Looye, D. Moormann, A. Varga, and S. Bennani, "Post-design stability robustness assessment of the rcam controller design entries," GARTEUR, Tech. Rep., 1997.

[6] G. Puyou and Y. Losser, "Clearance benchmark for a civil aircraft," in *Optimization-Based Clearance of Flight Control Laws: A Civil Aircraft Application*, A. Varga, A. Hansson, and G. Puyou, Eds. Springer Berlin Heidelberg, 2012, pp. 11–36.

[7] H.-D. Joos, "Worst-case parameter search based clearance using parallel nonlinear programming methods," in *Optimization-Based Clearance of Flight Control Laws: A Civil Aircraft Application*, A. Varga, A. Hansson, and G. Puyou, Eds. Springer Berlin Heidelberg, 2012, pp. 149–159.

[8] M. Hepperle, "Aerodynamic design and analysis - hap-omega-6," Institute of Aerodynamics and Flow Technology, German Aerospace Center (DLR), Tech. Rep., 2022.

[9] A. Voß, C. Koch, S. Niemann, V. Handojo, and C. Weiser, "Transition from preliminary to detailed design of a highly elastic solar electric aircraft," in *International Forum on Aeroelasticity and Structural Dynamics (IFASD)*, 2022.

[10] Y. J. Hasan, M. S. Roeser, M. Hepperle, S. Niemann, A. Voß, V. Handojo, and C. Weiser, "Flight mechanical analysis of a solar-powered high-altitude platform," *CEAS Aeronautical Journal*, vol. 14, no. 1, pp. 201–223, Nov. 2022.

[11] M. R. Waszak and D. K. Schmidt, "Flight dynamics of aeroelastic vehicles," *Journal of Aircraft*, vol. 25, no. 6, pp. 563–571, Jun. 1988.

[12] T. M. Kier, G. Looye, and J. Hofstee, "Development of aircraft flight loads analysis models with uncertainties for pre-design studies," in *Proc. of IFASD 2005,*

International Forum on Aeroelasticity and Structural Dynamics, 2005.

[13] R. L. Bisplinghoff, H. Ashley, and R. L. Halfman, *Aeroelasticity*. Dover Publications, Incorporated, 2013.

[14] *AS94900 Vehicle Management Systems - General Specification Guide for Flight Control Function, Design, Installation and Test of Piloted Military Aircraft*, SAE International Std., 2018.

[15] Volz Servos, *DA26 Technical Specification*, 2022.

[16] European Aviation Safety Agency (EASA), "Certification Specifications and Acceptable Means of Compliance for Large Aeroplanes CS-25," 2023.

[17] A. Voß, "HAP Design Load Assumptions," DLR-AE, techreport HAP-P030300-V5-R-L1, 2024.

[18] S. Schulz and D. Ossmann, "Estimation of global structural aircraft loads due to atmospheric disturbances for structural fatigue estimation," in *International Forum on Aeroelasticity and Structural Dynamics (IFASD)*, 2022.

[19] F. M. Hoblit, *Gust Loads on Aircraft: Concepts and Applications*. American Institute of Aeronautics and Astronautics, Jan. 1988.

[20] U.S. Department of Defense (DoD), "MIL-HDBK-1797: Flying Qualities of Piloted Aircraft," 2004.

[21] A. Varga, "Optimisation-based clearance," in *Advanced Techniques for Clearance of Flight Control Laws*, C. Fielding, A. Varga, S. Bennani, and M. Selier, Eds. Springer Berlin Heidelberg, 2002, pp. 107–117.

[22] H.-D. Joos, "A multiobjective optimisation-based software environment for control systems design," in *Proceedings. IEEE International Symposium on Computer Aided Control System Design*, 2002, pp. 7–14.

[23] K. Deb, A. Pratap, S. Agarwal, and T. Meyarivan, "A fast and elitist multiobjective genetic algorithm: Nsga-ii," *IEEE Transactions on Evolutionary Computation*, vol. 6, no. 2, pp. 182–197, 2002.

BIOGRAPHY

Christian Weiser *received his B.Sc. in engineering science and M.Sc. in aerospace engineering from Technical University Munich (TUM). Currently, he is employed as a Research Associate in the Flight Control and Simulation group at the German Aerospace Center (DLR) in Oberpfaffenhofen, Germany, with a focus on the application of robust control methods. His research since 2020 has focused on the flight control design and clearance for lightweight and very flexible High Altitude Long Endurance aircraft.*